JPE 19-4-11

https://doi.org/10.6113/JPE.2019.19.4.956
ISSN(Print): 1598-2092 / ISSN(Online): 2093-4718

Virtual Signal Injected MTPA Control for DTC Five-Phase IPMSM Drives

Guohai Liu[*], Yuqi Yang[*], and Qian Chen[†]

[†,*]School of Electrical and Information Engineering, Jiangsu University, Zhenjiang China

Abstract

This paper introduces a virtual signal injected maximum torque per ampere (MTPA) control strategy for direct-torque-controlled five-phase interior permanent magnet synchronous motor (IPMSM) drives. The key of the proposed method is that a high frequency signal is injected virtually into the stator flux linkage. Then the responding stator current is calculated and regulated to compensate the amplitude of the flux linkage. This is done according to the relationship between the stator current and the stator flux linkage. Since the proposed method does not inject any real signals into the motor, it does not cause any of the problems associated with high-frequency signals, such as additional copper loss and extra torque ripple. Simulation and experimental results are offered to verify the effectiveness of the proposed method.

Key words: Direct torque control (DTC), Five-phase interior permanent magnet synchronous motor (IPMSM), Maximum torque per ampere (MTPA), Virtual signal injection (VSI)

I. INTRODUCTION

Interior permanent magnet motors (IPMSMs) have been widely used in a variety of industrial applications due to their high power density, high efficiency, high reliability and wide constant power operating range [1]-[3]. With the development of modern power electronics conversion technologies and computer control theory, multiphase motor driving systems have experienced rapid development. When compared with three-phase interior permanent magnet synchronous motors, multiphase motors have higher power density, reliability and fault-tolerant performance [4]. In addition, they are a better fit for aerospace, ship electric propulsion, electric vehicles, etc.

To achieve better performance for motor driving, maximum torque per ampere (MTPA) control strategies are often used. The MTPA control strategy was initially proposed in field-oriented-control (FOC) with the goal of delivering the same electromagnetic torque with the minimum current amplitude. The existing MTPA control strategies can be divided into three main types, mathematical model based methods, lookup-table (LUT) based methods and extremum seeking methods. In [5]-[7], the MTPA points were calculated directly with constant parameters. However, these parameters may change due to the influence of cross-saturation, magnetic saturation and temperature in practical application [8], [9]. To solve this problem, researchers adopted online parameter estimation algorithms in [10], [11] to improve the accuracy of MTPA tracking. However, estimation accuracy affect the MTPA tracking performances. In addition, the cross-saturation effect is not considered. LUT-based methods are employed in [12]-[14] for MTPA tracking. In this method, LUT data can be acquired by simulations or numerical analysis. However, its accuracy is affected by manufacturing error, variations of material characteristics and temperature in real application. To improve the accuracy of the algorithm, LUT data can be obtained by a series of experiments. However, this method is quite time consuming and resource consuming. In addition, it is impractical to test these data in every different motors. Therefore, the application scope of LUT-based methods are greatly limited.

Extremum seeking control strategies, which can also be called online-search-based MTPA control strategies [15], including the signal injection based MTPA control schemes [16]-[18], reach MTPA point by adjusting current angle through disturbance. These methods are parameter independent.

Manuscript received Oct. 15, 2018; accepted Feb. 23, 2019
Recommended for publication by Associate Editor Gaolin Wang.
[†]Corresponding Author: chenqian0501@ujs.edu.cn
Tel: +86-15252900600, Fax: +86-51188787773, Jiangsu University
[*]School of Electronical and Information Eng., Jiangsu University, China

However, the dynamic performance of search algorithm is relatively poor because the convergence rate is slow. Additionally, the signal-injection-based MTPA control strategies result in additional copper losses and torque ripple due to the real signal injected into the motor. The recently proposed virtual-signal-injection-based MTPA control strategy [19] can realize the online search of the MTPA point by virtually injecting a high frequency into the torque equation mathematically. Therefore, it does not cause additional copper losses or torque ripple. However, this method is only realized under FOC.

When compared with FOC, direct torque control (DTC) has better torque dynamic performance. Therefore, it is therefore widely applied in industry servo applications. DTC was first proposed in three-phase induction motor drives [20]. However, it has since been extended to permanent magnet synchronous motors (PMSMs) and multiphase motors. However, research on using the MTPA control strategy for DTC drives is not as common as that for FOC drives. The main reasons are that DTC drives focus more on fast dynamic performance which fits industry servo applications better. In addition, the current is hardly controlled in DTC drives. However, many emerging applications (like mining and steel industries) require more and more energy source. The MTPA control strategy, which can improve system efficiency, is of great demand.

Conventional DTC drives usually set the reference flux linkage to a fixed value, such as the permanent magnetic flux. To maintain a constant value, the stator current often contains more reactive power components, which increases the copper loss and reduces the motor efficiency. In [21], the best-efficiency stator flux linkage reference is found offline, which can give the optimal flux linkage via a different torque and speed. However, this LUT-based method requires a massive amount of offline work and considerable hardware resources. An MTPA control strategy based on signal injection was proposed in [16]. This method can realize the online optimization of the reference flux linkage and motor parameters are not required. However, it causes extra copper losses and torque ripple due to the injected signal.

In this paper, a new virtual signal injected MTPA control strategy is proposed for five-phase IPMSM drives. The high frequency signal is injected into the flux linkage amplitude mathematically and the resonant current is calculated and analyzed. This method does not cause additional copper losses or the resonant problems associated with real signal injection since it does not injects any real signals into the motor.

The organization of this paper is as follows. The relationship between the stator current amplitude and the stator flux linkage amplitude is analyzed in Section II. The proposed virtual signal injected MTPA algorithm is introduced in Section III. Simulation verifications are presented in Section IV. Experiments are implemented to verify the validity of the proposed VSI-MTPA algorithm in Section V. Finally, some conclusions are presented in Section VI.

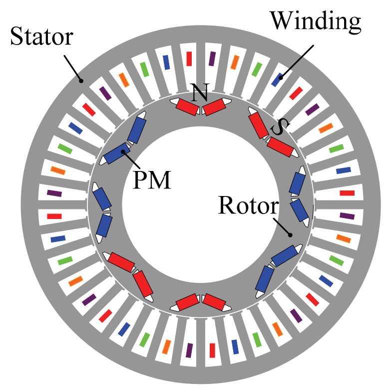

Fig. 1. Prototype of a five-phase IPMSM.

II. Relationship Between the Stator Current Amplitude and the Stator Flux Linkage Amplitude

Fig. 1 shows a five-phase IPMSM prototype with 40 slots and 8 poles. Unequal pole arcs and shifting pole-pairs are applied to lower the torque ripple [22].

For a five-phase IPMSM, torque expression without considering magnetic saturation is as follow:

$$T_e = \frac{5p}{2}[\psi_m i_q + (L_d - L_q) i_d i_q] \tag{1}$$

$$\begin{cases} i_d = |i_s|\cos(\beta) \\ i_q = |i_s|\sin(\beta) \end{cases} \tag{2}$$

Where i_d and i_q are the d-axis and q-axis currents, L_d and L_q are the d-axis and q-axis stator inductances, ψ_m is the flux linkage of the permanent magnet, p is the number of pole pairs, $|i_s|$ is the amplitude of the stator current, and β is the current vector angle.

From expression (1), the electromagnetic torque includes two parts. The former that is proportional to the q-axis current is the permanent magnet torque. The latter that is proportional to the product of the d-q axis currents is the reluctance torque. For the FOC, the MTPA point corresponds to the current angle β or d-axis current that can achieve the maximum torque for a given magnitude of current vector.

In the most common online-search-based MTPA algorithms (including signal-injection-based methods), the corresponding relation between the stator current magnitude and the current vector angle shown in Fig. 2 is used to judge the working condition of motors. As shown in Fig. 2, for current curves under a constant torque, the value of $d|i|/d\beta$ is zero at the lowest point of the curve, which corresponds to the MTPA point. When the current angle β is less than β_{MTPA}, the value of

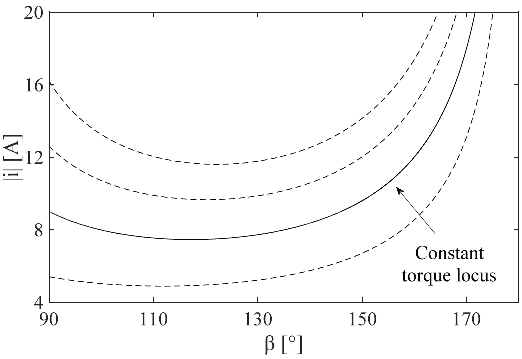

Fig. 2. Current amplitude locus with current angle under constant torque.

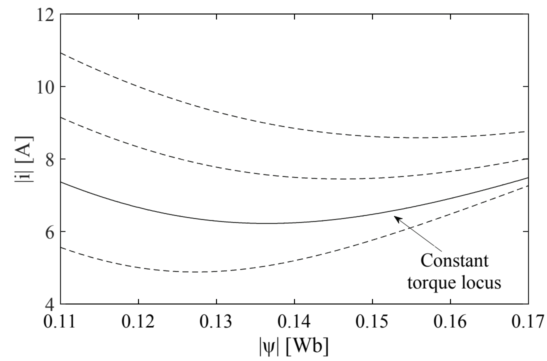

Fig. 3. Current amplitude locus with flux linkage amplitude under constant torque.

$d|i|/d\beta$ is negative, or it is positive. This feature can be used to estimate the working condition of the motor and to search for the MTPA point online.

However, in DTC drive systems, the current angles are not directly regulated. Instead, the flux linkage amplitudes are used to control the whole system. Therefore, the feature of the current β cannot be directly applied in DTC drive systems.

For the DTC, the torque expression (1) can be expressed as (3) in terms of the flux linkage with respect to the d-q reference frame.

$$T_e = \frac{5p}{2}(\psi_d i_q - \psi_q i_d) \tag{3}$$

$$\begin{cases} \psi_d = |\psi_s|\cos(\delta) = L_d i_d + \psi_m \\ \psi_q = |\psi_s|\sin(\delta) = L_q i_q \end{cases} \tag{4}$$

Where ψ_d and ψ_q are the d-axis and q-axis flux linkage amplitudes in the d-q reference frame, respectively, $|\psi_s|$ represents the amplitude of the stator flux linkage, and δ represents the angle of the flux linkage.

The stator current amplitude $|i_s|$ can be expressed by the flux linkage amplitude $|\psi_s|$ and the angle δ based on equation (4) as follows.

$$|i_s| = \sqrt{(\cos^2\delta / L_d^2 + \sin^2\delta / L_q^2)\psi_s - 2\psi_m \cos\delta\psi_s / L_d^2 + \psi_m^2 / L_d^2} \tag{5}$$

The relationship between the stator current and the stator flux linkage under the constant torque constrain can be obtained based on equations (1), (2) and (4). The result has been shown in Fig. 3. It can be seen that there exists a minimum in the objective function $|i_s|$ for a constant torque which corresponds to the MTPA point. The flux linkage amplitude opposite the MTPA point is the MTPA flux linkage amplitude ψ_{s_MTPA}. The value of $d|i_s|/d|\psi_s|$ is zero in the MTPA point. Therefore, the MTPA flux linkage amplitude ψ_{s_MTPA} can be calculated as follow by setting the value of $d|i_s|/d|\psi_s|$ to zero. The result is as follow:

$$\psi_{s\_MTPA} = \psi_m \cos\delta / (\cos^2\delta + \sin^2\delta (L_d / L_q)^2) \tag{6}$$

Equation (6) shows the optimal flux linkage amplitude which can achieve the minimum current amplitude for a constant torque, namely the MTPA point. However, the equation for ψ_{s_MTPA} contains three motor parameters. These parameters are the permanent magnet flux linkage ψ_m, and the inductances of d-axis and q-axis L_d and L_q. In real industrial applications, the motor parameters can change due to the change of motor working conditions. Therefore, the flux linkage amplitude provided by equation (6) may not be in accordance with the actual MTPA flux linkage amplitude.

As can be seen in Fig. 3, the corresponding relation between $|i|$ and $|\psi_s|$ is clear. The stator current amplitude $|i|$ decreases until it reaches the bottom. Then it increases with an increasing of the flux linkage amplitude $|\psi_s|$. That is to say, the value of $d|i_s|/d|\psi_s|$ is negative if $|\psi_s|$ is less than ψ_{s_MTPA}. Meanwhile, it is positive if $|\psi_s|$ is greater than ψ_{s_MTPA}. The slope, which is represented by $d|i_s|/d|\psi_s|$, approaches zero around the MTPA point.

These features can be used for MTPA tracking. The specific process of MTPA implementation will be introduced in the next section.

III. Proposed MTPA Procedure

A. Method to Obtain Current Variation Information

For a DTC drive system, the electromagnetic torque can be expressed as follows by substituting (4) into (3):

$$T_e = \frac{5p}{2}[\frac{1}{2}(\frac{1}{L_q} - \frac{1}{L_d})|\psi_s|\sin(2\delta) + \frac{\psi_m}{L_d}\sin(\delta)]|\psi_s| \tag{7}$$

Equation (7) represents the base equation of a DTC algorithm for a five-phase IPMSM. As can be seen from the equation, the torque is mainly decided by two variables, the flux linkage amplitude $|\psi_s|$ and the flux linkage angle δ in the d-q reference frame. In addition, the change of torque can be obtained by changing either of the two variables. A fast torque change can be obtained by varying the flux linkage angle δ, while variation of the flux linkage amplitude $|\psi_s|$ is usually used to change the operating region of the motor or to reach particular working conditions [16]. That is to say, the torque is mainly decided by the flux linkage angle δ, and the flux linkage amplitude $|\psi_s|$ has little effect. If a small high-frequency

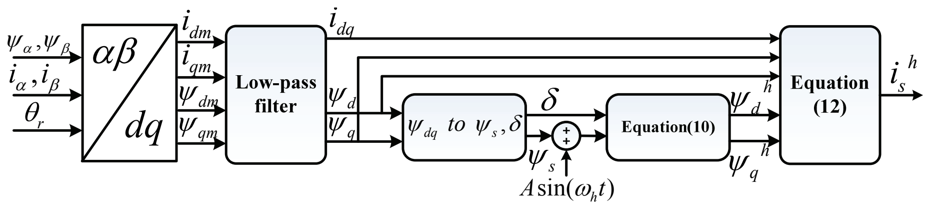

Fig. 4. Schematic of current amplitude variation calculation.

sinusoidal signal is added to the stator flux linkage amplitude, the torque fluctuates. However, the average torque is maintained as a stable value. Therefore, the torque can be assumed to be constant for a small high-frequency sinusoidal flux linkage amplitude variation.

The expression of the *d*-*q* axis current amplitude can be expressed by flux linkage amplitude in the *d*-*q* reference frame based on equation (8).

$$\begin{cases} i_d = (\psi_d - \psi_m)/L_d \\ i_q = \psi_q / L_q \end{cases} \tag{8}$$

The square of the stator current amplitude can be calculated with the *d*-*q* axis current amplitude as follow:

$$|i_s|^2 = i_d^{\,2} + i_q^{\,2} \tag{9}$$

By injecting a small signal into the stator flux linkage amplitude, the results of *d*-axis and *q*-axis flux linkage amplitude containing perturbation are as follow:

$$\begin{cases} \psi_d^{\,h} = (\psi_s + \Delta\psi_s)\cos\delta \\ \psi_q^{\,h} = (\psi_s + \Delta\psi_s)\sin\delta \end{cases} \tag{10}$$

Submitting (10) into (8), the corresponding *d*-axis and *q*-axis current after signal injection are as follows:

$$\begin{cases} i_d^{\,h} = (\psi_d^{\,h} - \psi_d)/L_d + i_d \\ i_q^{\,h} = (\psi_d^{\,h} i_q)/\psi_q \end{cases} \tag{11}$$

Combining (9) and (11), the resultant current amplitude variation can be expressed as follows:

$$|i_s^{\,h}| = \sqrt{[i_d + (\psi_d^{\,h} - \psi_d)/L_d]^2 + [(\psi_q^{\,h} i_q)/\psi_q]^2} \tag{12}$$

From equation (12), the sum current magnitude variation in (5) due to the injected signal can be acquired from the measured *d*-*q* axis current, *d*-*q* axis flux linkage amplitude and the *d*-*q* axis flux linkage amplitude containing perturbation given by (10). The *d*-axis inductance is also necessary. When compared to the three-parameter dependent equation (6), there is only one parameter L_d that is needed. The values of L_d can be acquired from corresponding LUTs or nominal values since the value of the *d*-axis inductance remains relatively steady during operation [14]. It can be found that the current amplitude variation can be extracted by mathematical signal injection instead of real signal injection. Therefore, the proposed method can be classified as a virtual-signal-injection based method.

Fig. 4 shows the specific flow of the current amplitude calculation processing based on virtual signal injection. The final current amplitude variation can be calculated based on $\psi_{\alpha\beta}$, $i_{\alpha\beta}$ and θ_r, which represent the α-β-axis flux linkage amplitude, α-β-axis current amplitude in stationary coordinates, and rotor position, respectively. The current and flux linkage of *d*-axis and *q*-axis components can be obtained with a rotation transformation. Both the current and flux linkage are low-pass filtered to cut down undesirable noise. The magnitude and angle of the flux linkage can be calculated with ψ_{dq}, and the high-frequency signal is then directly injected into the flux linkage amplitude. The flux linkage of *d*-axis and *q*-axis containing a high-frequency component can be calculated through equation (10) The final current amplitude variation can be obtained based on equation (12). It should be noticed that the rotor positions are used only in the virtual signal injection block and are not involved in the DTC loop. Therefore, the virtual signal injection block does not influence the DTC system and does not affect the inherent superiority of the DTC. For example, it does not affect the fast response of the torque.

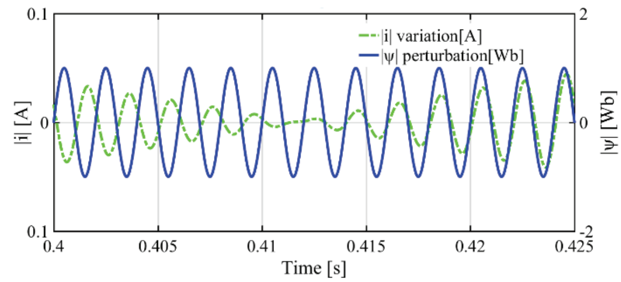

Fig. 5. Phase relationship between the $|i_s|$ and $|\psi_s|$.

From Section II, it is found that the MTPA point can be obtained by comparing the variations between $|\psi_s|$ and $|i_s|$. First, a sinusoidal signal is injected into the flux linkage amplitude $|\psi_s|$ shown in Fig. 4. The reference flux linkage amplitude is gradually increased from values less than the optimal flux linkage amplitude to values greater than the optimal flux linkage amplitude. Meanwhile, the current magnitude variation and the perturbation signal, A$\sin(\omega_h)t$, are required. In addition, they are filtered by the band-pass filter to extract the given frequency component. The results are shown in Fig. 5. At first, when the reference flux linkage amplitude is less than the optimal flux linkage amplitude, the resonant current is out of phase with the perturbation flux linkage. The resonant current becomes less relevant to the perturbation of the flux linkage when the reference flux linkage approaches the optimal one. Meanwhile, the phase relationship gets to be in phase when the reference flux linkage amplitude becomes greater than the

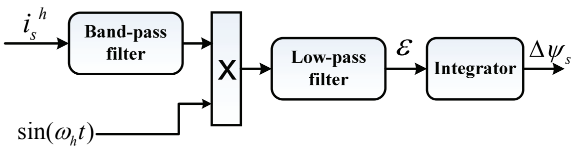

Fig. 6. Schematic of the signal processing block.

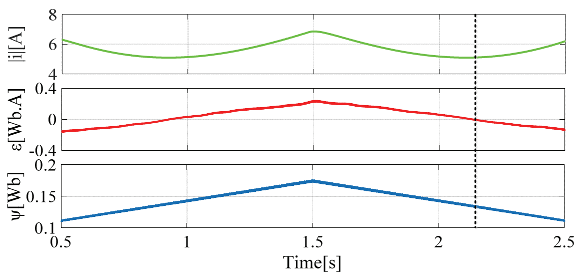

Fig. 7. Current magnitude, MTPA criterion value and reference flux linkage amplitude at a 6 Nm load torque.

optimal flux linkage amplitude. The current amplitude variation around the MPTA point is less than that of the other two cases. The injected signal frequency is 300 Hz. All of the above correspond to what was discussed in Section II, which proves the rationality of the proposed calculating method of current amplitude.

B. Signal Processing for the Extraction of the MTPA Criterion

When the perturbation is added into the flux linkage amplitude $|\psi_s|$, current amplitude with perturbation is as follow:

$$|i_s^h| = |i_s| + A\frac{d|i_s|}{d|\psi_s|}\sin(\omega_h t) + A^2\frac{d}{d|\psi_s|}\left(\frac{d|i_s|}{d|\psi_s|}\right)\sin^2(\omega_h t) + \cdots \quad (13)$$

$d|i_s|/d|\psi_s|$ can be extracted from current amplitude containing a high-frequency $|i_s^h|$ with the signal processing method shown in Fig. 6. A band-pass filter with a center frequency equal to the high-frequency injected is utilized to extract a specific frequency ω_h signal in $|i_s^h|$. Then the signal output of the band-pass filter is multiplied with $\sin(\omega_h t)$.

$$\begin{aligned} K\frac{d|i_s|}{d|\psi_s|}A\sin^2(\omega_h t) &= K\frac{d|i_s|}{d|\psi_s|}A\{\frac{1}{2}[\cos(0) - \cos(2\omega_h t)]\} \\ &= \frac{1}{2}KA\frac{d|i_s|}{d|\psi_s|} - \frac{1}{2}KA\frac{d|i_s|}{d|\psi_s|}\cos(2\omega_h t) \end{aligned} \quad (14)$$

$d|i_s|/d|\psi_s|$ can be extracted by a first-order low-pass filter whose cutoff frequency is below the frequency ω_h of the virtually injected signal. The output ε of the low-pass filter, which is proportional to $d|i_s|/d|\psi_s|$, is input to an integrator to obtain the compensation flux linkage amplitude of the reference value of the flux linkage amplitude.

Simulations on the change of the MTPA criterion value have also been implemented. The obtained results are shown in Fig. 7. At the same time, the current and flux amplitude waveforms are given. In Fig. 7, the dotted line represents the minimum current moment. The MTPA criterion value corresponding to the dotted line is about zero at the same time. It can also be

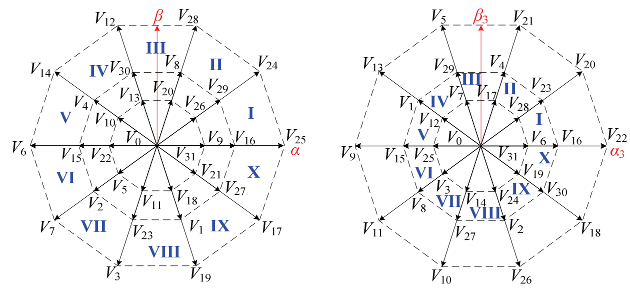

(a) (b)

Fig. 8. Voltage vector distributions. (a) Voltage vectors in the α-β frame. (b) Voltage vectors in the α_3-β_3 frame.

seen from Fig. 7 that when the reference flux linkage amplitude is less than the MTPA flux linkage amplitude, the criterion value is negative. Meanwhile, it is positive when the reference flux linkage amplitude is greater than the MTPA flux linkage amplitude. This is consistent with the conclusions shown in Section II and the results shown in Fig. 5.

C. Control System Configuration

When compared to three-phase IPMSMs, there exists high order harmonics in five-phase IPMSMs for it owns three dimensional subspaces [23]. To restrain high order harmonics, switch tables containing both α-β and α_3-β_3 reference frames have been used to improve the performance of IPMSMs [24].

Fig. 8 shows five-phase IPMSM space voltage vectors in both the α-β and α_3-β_3 frames. It can be found from Fig. 8 that the large voltage vector in the α-β frame becomes a small vector in the α_3-β_3 frame, the medium vector is still a medium vector in the α_3-β_3 frame, and the small vector becomes a large vector in the α_3-β_3 frame. In addition, the medium vector in the α-β frame is opposite that of the large vector and the small vector in the α_3-β_3 frame. This means that the effect on the flux linkage of the medium vector is opposite that of the large vector and the small vector in the α_3-β_3 frame. Therefore, appropriate selection of the medium voltage vector can guarantee both the controlled state of the torque and the flux linkage, and effectively suppress the magnitude of the flux linkage in the α_3-β_3 frame, which reduces the high order harmonics. According to the above analysis, new switch tables that consider both the α-β and α_3-β_3 frames have been proposed. These switch tables are shown in Table I and Table II.

Fig. 9 shows the control block diagram of a five-phase IPMSM drive containing the proposed VSI-MTPA algorithm. The fundamental torque control and flux linkage amplitude control loop are just the same as the conventional methods. The reference torque can be regulated by speed based on a PI controller just like the traditional one. The torque and the flux linkage estimator are shown in (15) and (16), respectively.

$$T_e = \frac{5}{2}p(\psi_\alpha i_\beta - \psi_\beta i_\alpha) \quad (15)$$

$$\begin{cases} \psi_\alpha = \int(u_\alpha - Ri_\alpha) \\ \psi_\beta = \int(u_\beta - Ri_\beta) \end{cases} \quad (16)$$

TABLE I
IMPROVED SWITCH TABLE IN THE *A*-*B* FRAME

$\Delta\psi$	ΔT_e	*z*									
		I	II	III	IV	V	VI	VII	VIII	IX	X
0	-1	7	8	9	10	2	2	3	4	5	6
0	0	11	0	11	0	11	0	11	0	11	0
0	1	5	6	7	8	9	10	1	2	3	4
1	-1	10	1	2	3	4	5	6	7	8	9
1	0	0	11	0	11	0	11	0	11	0	1
1	1	2	3	4	5	6	7	8	9	10	1

TABLE II
SWITCH TABLE IN THE *A*3-*B*3 FRAME

z	Sector of ψ_{s3}	Voltage Vector
1	4, 5, 6, 7, 8, 9, 10, 1, 2, 3	V_{16}, V_{25}
2	7, 8, 9, 10, 1, 2, 3, 4, 5, 6	V_{29}, V_{24}
3	10, 1, 2, 3, 4, 5, 6, 7, 8, 9	V_8, V_{28}
4	3, 4, 5, 6, 7, 8, 9, 10, 1, 2	V_{30}, V_{12}
5	6, 7, 8, 9, 10, 1, 2, 3, 4, 5	V_4, V_{14}
6	9, 10, 1, 2, 3 ,4 ,5, 6, 7, 8	V_{15}, V_6
7	2, 3, 4, 5, 6, 7, 8, 9, 10, 1	V_2, V_7
8	5, 6, 7, 8, 9, 10, 1, 2, 3, 4	V_{23}, V_3
9	8, 9, 10, 1, 2, 3, 4, 5, 6, 7	V_1, V_{19}
10	1, 2, 3, 4, 5, 6, 7, 8, 9, 10	V_{30}, V_{17}
0/11	1, 2, 3, 4, 5, 6, 7, 8, 9, 10	V_0, V_{31}

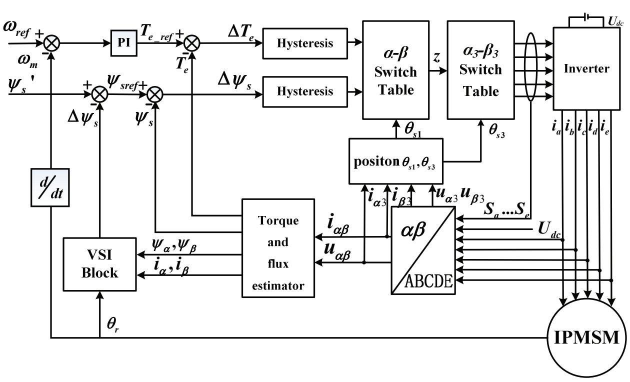

Fig. 9. Control block diagram of the proposed virtual signal injection.

Instead of giving a designated value, the reference flux linkage amplitude is compensated by a VSI block. The details of the VSI block are shown in Fig.4 and Fig.6, and discussed above.

It should be noticed that the convergence rate of the VSI block does no influence the fast response of DTC drives. In addition, the virtually injected signal does not affect the torque or current because it does not inject any real signals. Therefore, the frequency of the injected signal is easy to choose. In addition, the integral parameter, shown in Fig. 6, that decides the convergence rate of the flux linkage amplitude can also be set to a higher value to improve the dynamic performance.

IV. SIMULATION VERIFICATION

Simulations have been implemented and compared with a prototype five-phase IPMSM drive system to demonstrate the effectiveness of the proposed VSI-MTPA algorithm. The motor parameters are shown in Table III.

In the simulation, the sampling time of the DTC drive system is 1μs, the load torque is 4 Nm, and the speed is set to 300r/min. First, the MTPA flux linkage amplitude is tested and the final value is 0.132Wb. As shown in Fig. 10(a), the referenced flux linkage amplitude is set to 0.132Wb. Then, it steps to 0.111Wb at 0.4s. After 0.6s, the proposed VSI-MTPA control strategy is adopted. After the proposed VSI-MTPA control strategy is used, the stator flux linkage increases gradually and finally approaches 0.132Wb, which is the MTPA flux linkage amplitude under the given load torque. As shown in Fig. 10(b), the current amplitude steps from 3.6A to 4.5A when the flux linkage amplitude decreases from 0.132Wb to 0.111Wb. After the proposed MTPA strategy is adopted, the current amplitude gradually decreases and finally reaches its initial value. The torque shown in Fig. 10(c) fluctuates slightly at 0.4s due to current changes. The final torque becomes as stable as that before 0.4s. It can also be observed that the torque fluctuation is less than 10%. Moreover, there is no additional torque ripple after 0.6s since the proposed method is based on virtual signal injection. Variations of the MTPA criterion value shown in Fig. 10(d), correspond to what was discussed in Section III. The magnitude of $\Delta\psi_s$, shown in Fig. 10(e), corresponds to the compensation required for the stator flux linkage magnitude in Fig. 10(a). The speed performance is shown in Fig. 10(f). As shown in Fig. 10(f), the speed fluctuation is less than 1%. The speed fluctuates slightly at 0.4s due to the torque wave. Then it quickly recovers to the normal condition. Therefore, the algorithm can be shown to have no effect on the rotational speed performance. The simulation result in Fig. 10 shows that the proposed MTPA tracking method can quickly optimize the flux linkage amplitude to the MTPA value and that it does not cause extra torque ripple. The proposed method is shown to have excellent steady state performance.

As mentioned before, the proposed method is virtual-signal-injected based. In order to show this performance, FFT analyses of the flux linkage in the *α*-*β* coordinates for the constant flux linkage amplitude algorithm and the VSI-MTPA algorithm have been provided in Fig. 11. The fundamental value is equal to one. The fundamental frequency is 20Hz, and the injected signal frequency is 150Hz. The THD is 1.23% for the constant flux linkage amplitude algorithm and 0.99% for the VSI-MTPA algorithm. From Fig. 11, it can be seen that the harmonic proportion of the VSI-MTPA algorithm is basically the same as that of the constant flux amplitude algorithm, which demonstrates that the proposed VSI-MTPA algorithm does not cause extra harmonics.

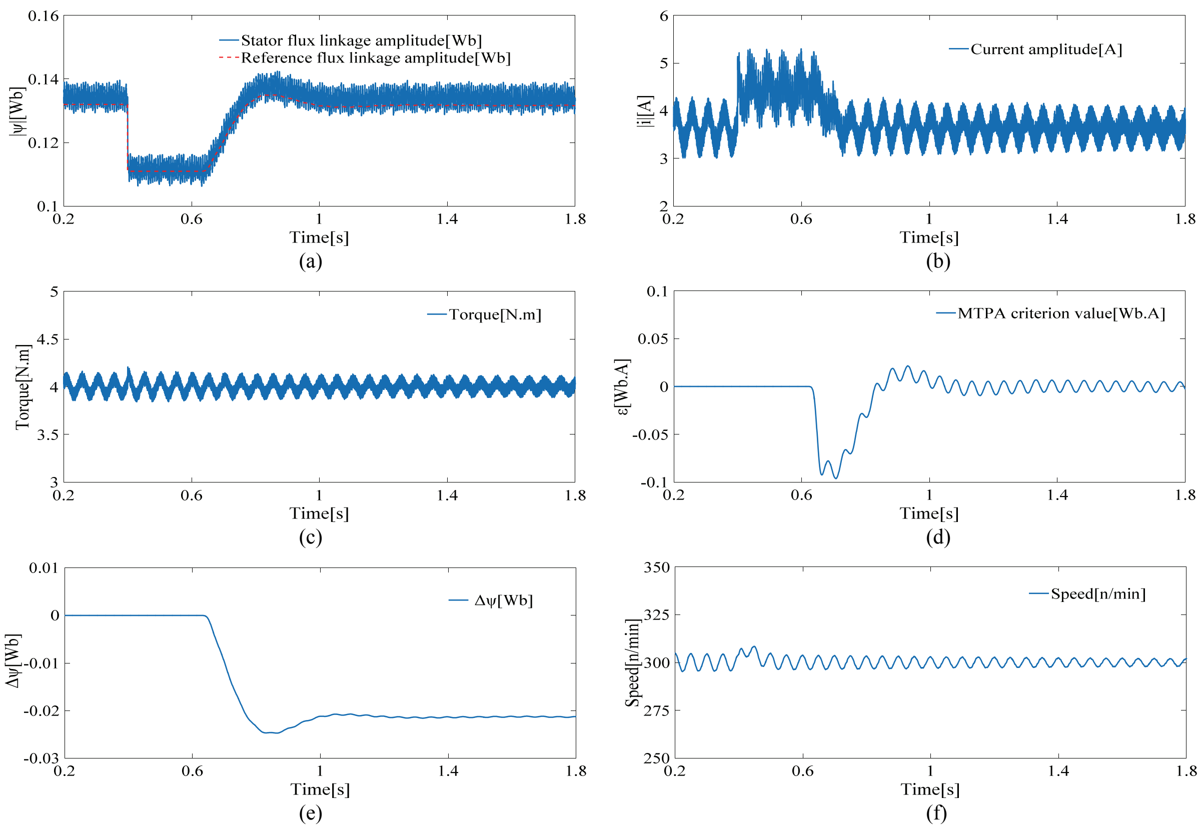

Fig. 10. Simulated results. (a) Stator flux linkage amplitude and reference flux linkage amplitude tracking performance. (b) Variation of the stator current amplitude. (c) Variation of the electromagnetic torque. (d) Variation of the MTPA criterion value. (e) Variation of $\Delta\psi_s$. (f) Locus of the speed.

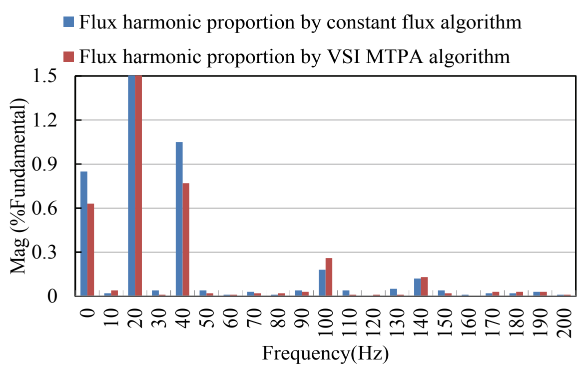

Fig. 11. Comparison of the α-β flux linkage harmonic proportion by the constant flux amplitude algorithm and the VSI MTPA algorithm.

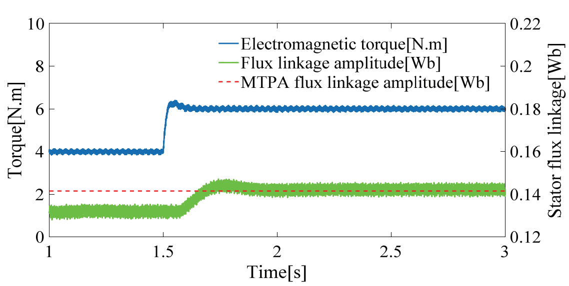

Fig. 12. Stator flux linkage and electromagnetic torque tracking response to the load step.

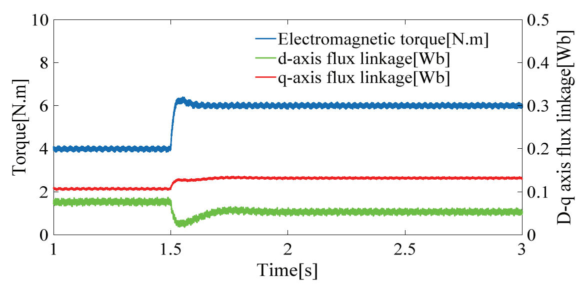

Fig. 13. Flux linkages in the d-q coordinate tracking response to the load step.

Fig. 12 shows simulation results of the torque and flux linkage amplitude for load torque step. The ideal MTPA flux linkage amplitude value at 6 Nm is shown with dotted line. From Fig. 12, the proposed VSI-MTPA algorithm show good tracking performance for load step. It can be concluded that the proposed method has excellent dynamic performance. Detailed flux linkages in the d-q coordinate are shown in Fig. 13. It can be seen that the d-q flux linkages have a fast response to load steps. Fig. 14 shows the trajectories of currents in the d-q coordinates. The dotted line represents the MTPA d-axis current at 6Nm. It can be seen that the currents in the d-q coordinates can response to the load step and show good accuracy in tracking the theoretical MTPA d-axis current.

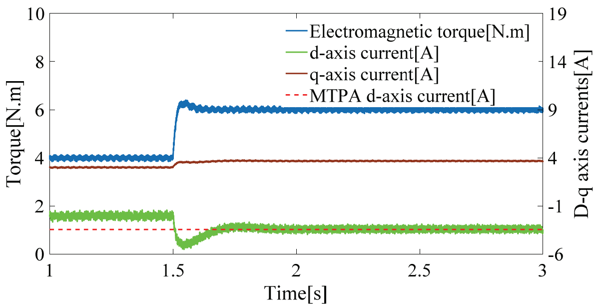

Fig. 14. Currents in the *d-q* coordinate tracking response to the load step.

V. Experiment Verification

To verify the feasibility of the proposed VSI-MTPA algorithm for DTC drive systems, corresponding test platform has been built. The platform is shown in Fig. 15. The experimental platform includes a five-phase IPMSM, a five-phase inverter, and a magnetic powder brake. A dSPACE1005 controller is used to implement the whole algorithm. The torque is measured by a high precision torque sensor (YH502/20Nm). The sample rate of the sampling circuit is 10 kHz, and the given DC voltage is 80 V. In this experiment, the frequency of the injected signal in the VSI block is 150 Hz.

Fig. 16 shows torque and current waveforms from the constant flux linkage amplitude algorithm to the VSI based MTPA algorithm. The dotted line represents the algorithm switching point. The current waveform is a bit distorted due to high order harmonics. Although a harmonic suppression method is employed, there are still some other high order harmonics, which deteriorate the current performance. However, the MTPA method itself effectively reduces the current amplitude after the algorithm switching. Meanwhile, it also keeps the average value of the torque constant at 4 Nm before and after switching. The value of the current amplitude remains at 4.6A with the constant flux linkage amplitude algorithm and decreases to 3.7A after the algorithm is switched to the proposed VSI-MTPA method. The current amplitude declined by 0.9A, while the torque remained constant, which demonstrates the function of the proposed method.

Fig. 17 shows waveform of the speed and the *d-q* axis currents for algorithm switching. From Fig. 17, the speed fluctuation is 2.7%. The speed of the motor is kept stable during the algorithm switch period, and the *d-q* axis currents change quickly to track to the MTPA trajectory.

Fig. 18 shows the *d-q* axis flux linkage amplitudes trajectories for algorithm switching. The *d-q* axis flux linkages change quickly after the algorithm is switched from the constant flux linkage magnitude to the VSI-MTPA algorithm. Fig. 17 and Fig. 18 prove that the proposed method is effective for MTPA tracking and that it does not effect the speed performance.

TABLE III
Parameters of the IPMSM

Pole-pairs	4
Fundamental PM flux linkage	0.111Wb
Phase resistance	0.8Ω
D-axis inductance	17mH
Q-axis inductance	36mH
Rated torque	12Nm
Rated current	10.8A
Rated speed	1000r/min

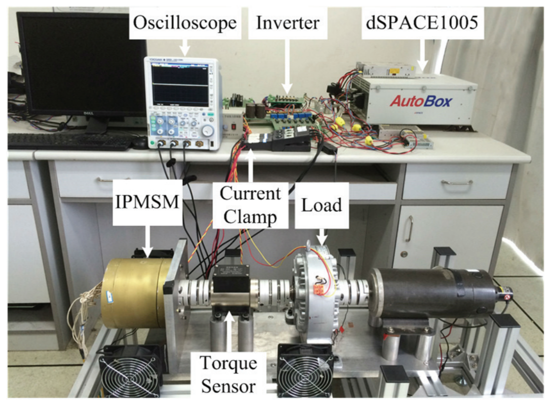

Fig. 15. Experimental platform.

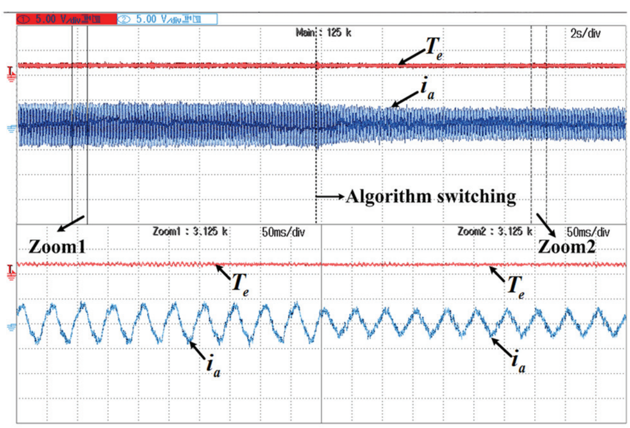

Fig. 16. Torque and currents waveforms from the constant flux linkage amplitude algorithm to the VSI-MTPA operation.

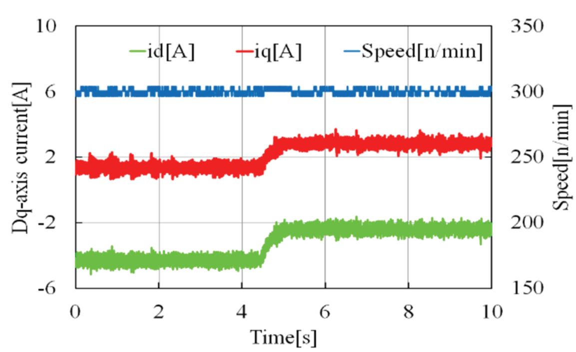

Fig. 17. Trajectories of the speed and *d-q* axis currents for algorithm switching.

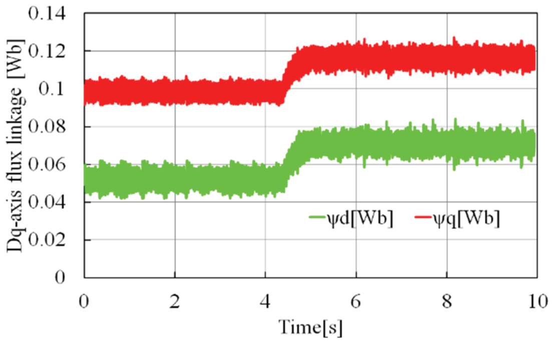

Fig. 18. Trajectories of the *d*-*q* axis flux linkage amplitudes for algorithm switching.

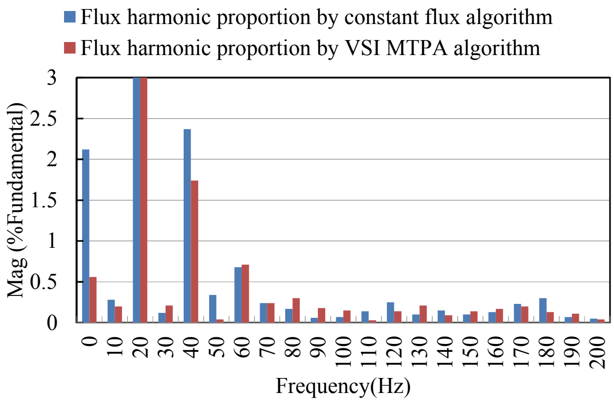

Fig. 19. Comparison of the α-β flux linkage harmonic proportion by the constant flux amplitude algorithm and the VSI-MTPA algorithm.

Experiment for the comparisons of the α-β flux linkage harmonic proportion by the constant flux amplitude algorithm and the VSI-MTPA algorithm have been implemented. The results are shown in Fig. 19. The fundamental value is equal to one. The fundamental frequency is 20Hz, and the frequency of the injected signal is 150Hz. The THD is 2.76% for the constant flux linkage amplitude algorithm, and 2.05% for the VSI-MTPA algorithm. From Fig. 19, the harmonic proportion of the VSI-MTPA algorithm is basically the same as that of constant flux amplitude algorithm. Therefore, it can be demonstrated that no actual injection signal occurs in the proposed method.

Experiments on the corresponding relations for the current magnitude, the stator flux linkage amplitude and the MTPA criterion value have been implemented. The results are shown in Fig. 20. When the reference flux linkage amplitude varies from 0.111Wb to 0.17Wb, the minimum values of the current amplitude correspond to the zero point of ε, which is in accordance with the content discussed in Section III. The feasibility of the algorithm is verified in principle by the experiment. After 30s, the proposed algorithm is used. The values of $|i|$, ε and $|\psi_s|$ step to 5.2A, 0 and 0.145Wb, respectively. All three of these parameters step quickly because the compensation of the flux linkage amplitude reached the

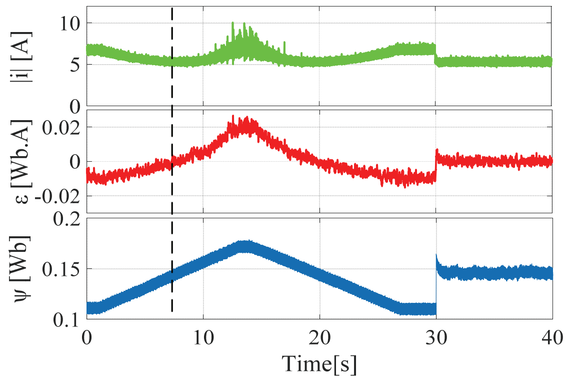

Fig. 20. Corresponding relations for the current amplitude, MTPA criterion value and flux linkage amplitude at a 6 Nm load torque.

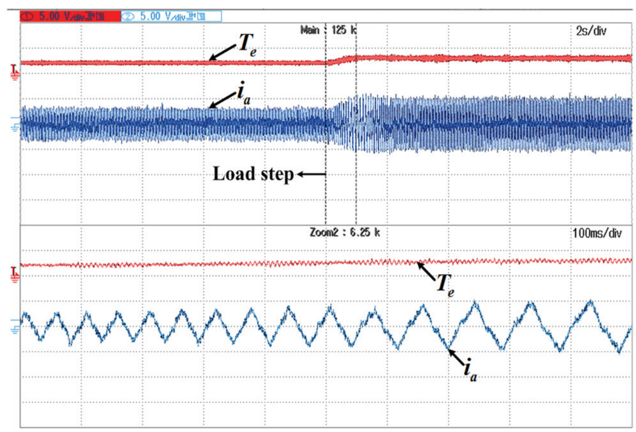

Fig. 21. Torque and currents waveforms during a load step for the VSI based MTPA algorithm.

MTPA compensation value before 30s. Then the values of the three parameters step according to the MTPA value when the algorithm is used. From the current amplitude $|i|$ and the ε trajectory, it is clear that the final current amplitude adjusted by the proposed VSI-MTPA is equal to the minimum values from before 30s. In addition, ε fluctuates around zero which means that it is a MTPA point. Therefore, the proposed method can be shown to accurately track the MTPA flux linkage amplitude. The experimental results are basically the same as the simulated ones. There are some small errors in the numerical values due to the simulated model errors, and manufacturing and measuring errors of the motor. However, both the simulations and experimental results demonstrate the accuracy of the proposed algorithm.

Fig. 21 shows waveforms of the torque and currents corresponding to a load step for the VSI-MTPA algorithm. It can be seen that both the electromagnetic torque and current of phase-A change quickly to a step change in the torque, which shows the good dynamic performance of the proposed algorithm. In addition, both the torque and current can maintain relative stability during the load step, which demonstrates the stability of the transient state of the VSI-MTPA algorithm.

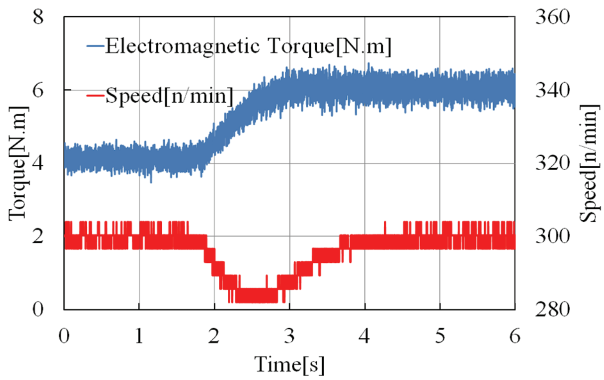

Fig. 22. Trajectories of electromagnetic torque and speed for step change in torque.

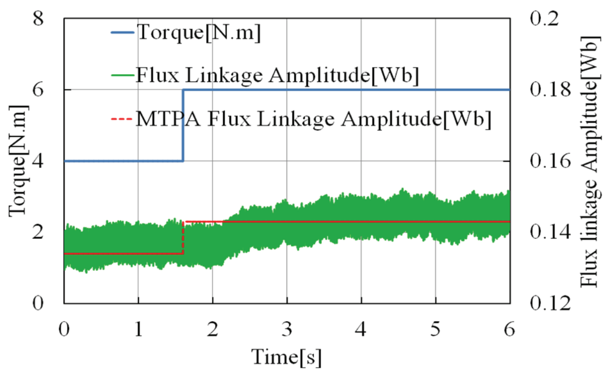

Fig. 23. Stator flux linkage amplitude tracking response to step change in torque.

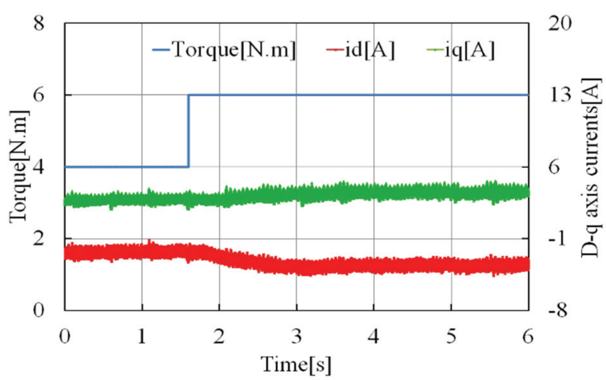

Fig. 24. Trajectories of *d-q* axis currents to step change in torque.

Fig. 22 shows the trajectories of electromagnetic torque and speed for a step change in torque. In Fig. 22, the electromagnetic torque changes quickly with the load step. The speed only fluctuates when the load steps, and it is quickly restored to its initial stable state within 2s. Fig. 23 shows the flux linkage tracking response to a step change in torque. The dotted line represents the theoretic MTPA flux linkage amplitude. It can be seen that the stator flux linkage amplitude changes quickly with the load step and that it accurately tracks the theoretical MTPA value. Fig. 24 and Fig. 25 show the trajectories of the *d-q* axis currents and the *d-q* axis flux linkage amplitudes to a step change in torque, where

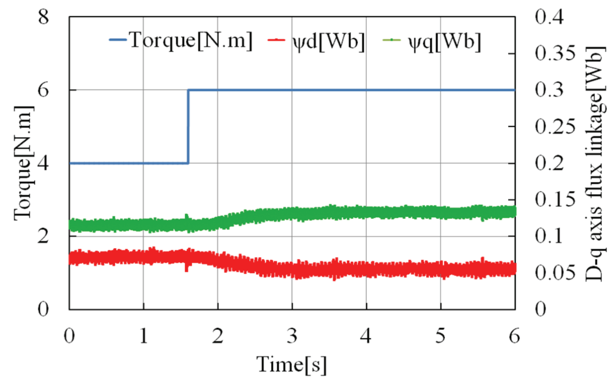

Fig. 25. Trajectories of the *d-q* axis flux linkages to a step change in torque.

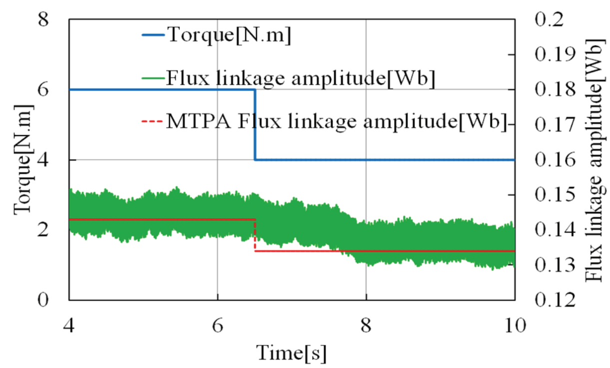

Fig. 26. Stator flux linkage amplitude tracking response to a step reduction in torque.

both the *d-q* axis currents and the *d-q* axis flux linkage amplitudes respond well to the load step. The obtained experimental results are also consistent with the simulated results. Although there are some small errors in the numerical values due to manufacturing and measuring errors, both the simulations and experimental results demonstrate the dynamic performance of the proposed algorithm. Fig. 26 shows the stator flux linkage amplitude tracking response to a step reduction in torque. It is obvious that the stator flux amplitude can still accurately track the theoretical MTPA value for load reduction. From Fig. 21 to Fig. 26, the proposed algorithm has been shown to possess excellent dynamic performance and good tracking accuracy.

Fig. 27 shows the trajectories of the speed and the *d-q* axis currents to a step change in speed. It is clear that the speed have a good performance for speed step. The *d-q* axis currents fluctuate when the speed steps and is quickly restored to its original value. Fig. 28 shows the trajectories of the speed and the stator flux linkage amplitude corresponding to a step change in speed. The stator flux linkage amplitude fluctuates when the speed steps and is restored to its original value from before the speed step. Both Fig. 27 and Fig. 28 show that the algorithm has a good speed dynamic performance and that the tracking of the currents or stator flux linkage amplitudes are independent of speed.

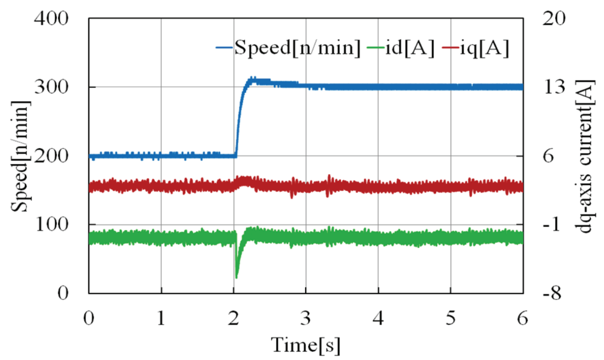

Fig. 27. Trajectories of the speed and *d*-*q* axis currents to a step change in speed.

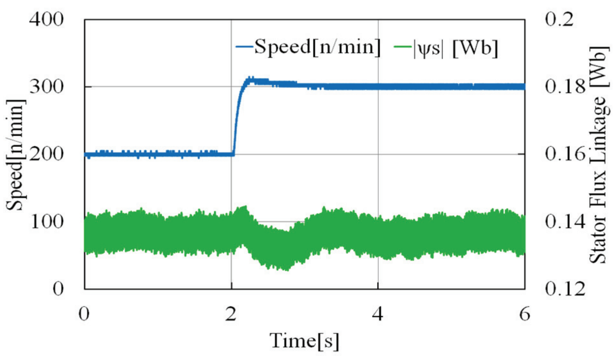

Fig. 28. Trajectories of speed and stator flux linkage to a step change in speed.

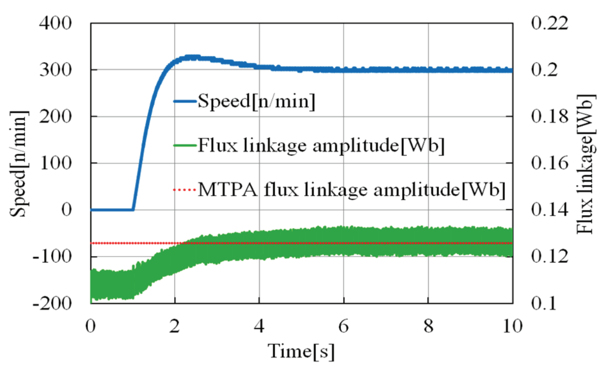

Fig. 29. Starting performance of the proposed MTPA algorithm at a 2Nm load torque.

Fig. 29 shows the starting performance of the proposed VSI-MTPA algorithm. The referenced speed is set as 300r/min, and the load torque is set as 2Nm. It can be seen that the proposed MTPA algorithm can quickly and accurately realize the load starting and track the MTPA point. As can be seen in both the torque and speed step experiments, all of the variables stay relative stable during the transient state. It can be concluded that the proposed method has a good stability for the transient state.

From both the simulations and experimental results, the proposed method is shown to be effective for MTPA tracking and has a good accuracy for the seeking of the MTPA stator flux linkage amplitude. It should be noted that the VSI-MTPA algorithm has universal applicability since the formulas used to derive the algorithm can be used on all motors. Therefore, the algorithm can also be applied to other motors such as three-phase motors.

Although the experiment results have demonstrated the validity of the proposed method, it has some limitations. The value of the *d*-axis inductance is needed for the MTPA calculations. In addition, there are some fluctuations in the speed, flux and currents. However, these fluctuations can be reduced by new modulation methods, e.g. SVPWM [25].

VI. Conclusion

In this paper, an online MTPA tracking algorithm for DTC-based five-phase IPMSM drives has been proposed. The proposed method is VSI based and it mathematically injects a high frequency signal into the flux linkage amplitude of a DTC drive. MTPA points are obtained by using the relationship between the current magnitude and the stator flux linkage amplitude. Since this method does not inject any real signals, it does not result in additional copper loss or torque ripple when compared to real-signal-injection based methods. Simulations and experiments have been implemented to verify the proposed algorithm. These results demonstrate that the proposed method have a good performance for MTPA tracking.

References

[1] G. Wang, L. Yang, B. Yuan, B. Wang, G. Zhang, and D. Xu, “Pseudo-random high-frequency square-wave voltage injection based sensorless control of IPMSM drives for audible noise reduction,” *IEEE Trans. Ind. Electron.*, Vol. 63, No. 12, pp. 7423-7433, Dec. 2016.

[2] Y. Kano, “Torque ripple reduction of saliency-based sensorless drive concentrated-winding IPMSM using novel flux barrier,” *IEEE Trans. Ind. Appl.*, Vol. 51, No. 4, pp. 2905-2916, Jul./Aug. 2015.

[3] M. M. I. Chy and M. N. Uddin, “Development and implementation of a new adaptive intelligent speed controller for IPMSM drive,” *IEEE Trans. Ind. Appl.*, Vol. 45, No. 3, pp. 1106-1115, May/Jun. 2009.

[4] Q. Chen, W. Zhao G. Liu, and Z. Lin, “Extension of virtual-signal-injection-based MTPA control for five-phase IPMSM into fault-tolerant operation” *IEEE Trans. Ind. Electron.*, Vol: 66, No. 2, pp. 944-955, Feb. 2019.

[5] T. M. Jahns, G. B. Kliman, and T. W. Neumann, “Interior permanent magnet synchronous motors for adjustable-speed drives,” *IEEE Trans. Ind. Appl.*, Vol. IA-22, No. 4, pp. 738-747, Jul. 1986.

[6] S. Morimoto, M. Sanada, and Y. Takeda, “Wide-speed operation of interior permanent magnet synchronous motors with high-performance current regulator,” *IEEE Trans. Ind. Appl.*, Vol. 30, No. 4, pp. 920-926, Jul./Aug. 1994.

[7] M. N. Uddin, T. S. Radwan, and M. A. Rahman, “Performance of interior permanent magnet motor drive over wide speed range,” *IEEE Trans. Energy Convers.*, Vol. 17, No. 1, pp. 79-84, Mar. 2002.

[8] H. W. Lee, K.-D. Lee, W.-H. Kim, I.-S. Jang, M.-J. Kim, J.-J. Lee, and J. Lee, "Parameter design of IPMSM with concentrated winding considering partial magnetic saturation," *IEEE Trans. Magn.*, Vol. 47, No. 10, pp. 3653-3656, Oct. 2011.
[9] X. Liu, H. Chen, J. Zhao, and A. Belahcen, "Research on the performances and parameters of interior PMSM used for electric vehicles," *IEEE Trans. Ind. Electron.*, Vol. 63, No. 6, pp. 3533-3545, Jun. 2016.
[10] R. Ni, D. Xu, G. Wang, L. Ding, G. Zhang, and L. Qu, "Maximum efficiency per ampere control of permanent-magnet synchronous machines," *IEEE Trans. Ind. Electron.*, Vol. 62, No. 4, pp. 2135-2143, Apr. 2015.
[11] P. Niazi, H. A. Toliyat, and A. Goodarzi, "Robust maximum torque per ampere (MTPA) control of PM-assisted SynRM for traction applications," *IEEE Trans. Veh. Technol.*, Vol. 56, No. 4, pp. 1538-1545, Jul. 2007.
[12] T. M. Jahns, G. B. Kliman, and T. W. Neumann, "Interior permanent-magnet synchronous motors for adjustable-speed drives," *IEEE Trans. Ind. Appl.*, Vol. IA-22, No. 4, pp. 738-747, Jul. 1986.
[13] A. Consoli, G. Scarcella, G. Scelba, and A. Testa, "Steady-state and transient operation of IPMSMs under maximum-torque-per-ampere control," *IEEE Trans. Ind. Appl.*, Vol. 46, No. 1, pp. 121-129, Jan./Feb. 2010.
[14] S. Y. Jung, J. Hong, and K. Nam, "Current minimizing torque control of the IPMSM using Ferrari's method," *IEEE Trans. Power Electron.*, Vol. 28, No. 12, pp. 5603-5617, Dec. 2013.
[15] R. S. Colby and D. W. Novotny, "An efficiency-optimizing permanent magnet synchronous motor drive," *IEEE Trans. Ind. Appl.*, Vol. 24, No. 3, pp. 462-469, May/Jun. 1988.
[16] S. Bolognani, L. Peretti, and M. Zigliotto, "Online MTPA control strategy for DTC synchronous-reluctance-motor drives," *IEEE Trans. Power Electron.*, Vol. 26, No. 1, pp. 20-28, Jan. 2011.
[17] G. Liu, J. Wang, W. Zhao, and Q. Chen, "A novel MTPA control strategy for IPMSM drives by space vector signal injection," *IEEE Trans. Ind. Electron.*, Vol. 64, No. 12, pp. 9243 - 9252, Dec. 2017.
[18] R. Antonello, M. Carraro, and M. Zigliotto, "Maximum-torque-per-ampere operation of anisotropic synchronous permanent-magnet motors based on extremum seeking control," *IEEE Trans. Ind. Electron.*, Vol. 61, No. 9, pp. 5086-5093, Sep. 2014.
[19] T. Sun, J. Wang, and X. Chen, "Maximum torque per ampere (MTPA) control for interior permanent magnet synchronous machine drives based on virtual signal injection," *IEEE Trans. Power Electron.*, Vol. 30, No. 9, pp. 5036-5045, Sep. 2015.
[20] I. Takahashi and T. Noguchi, "A new quick-response and high-efficiency control strategy of an induction motor," *IEEE Trans. Ind. Appl.*, Vol. IA-22, No. 5, pp. 820-827, Sep. 1986.
[21] J. Habibi and S. Vaez.-Zadeh, "Efficiency-optimizing direct torque control of permanent magnet synchronous machines," in *Proc. IEEE Power Electron. Spec. Conf. (PESC)*, pp. 759-764, 2005.
[22] Q. Chen, G. Xu, W. Zhao, L. Liu, and Z. Lin, "Torque ripple reduction in five-phase IPM motors by lowering interactional MMF" *IEEE Trans. Ind. Electron.*, Vol. 65, No. 11, pp. 8520-8531, Nov. 2018
[23] L. Parsa and H. A. Toliyat, "Sensorless Direct torque control of five-phase interior permanent-magnet motor drives," *IEEE Trans. Ind. Appl.*, Vol. 43, No. 4, pp. 952-959, Jul. 2007.
[24] X. Huang, G. Liu, H. Zhou, and J. Ji, "Direct thrust control for five-phase tubular linear PM motor based on third-harmonic current suppression" in *Proc. Int. Conf. Electr. Mach. Syst.* (*ICEMS*), pp.1-4, 2017.
[25] F. Yu, X. Zhang, M. Qiao, and C. Du, "The direct torque control of multiphase permanent magnet synchronous motor based on low harmonic space vector PWM," in *Proc. IEEE Int. Conf. Ind. Technol.*, pp.1-5, 2008.

Guohai Liu (M'07–SM'15) received his B.S. degree from Jiangsu University, Zhenjiang, China, in 1985. He received his M.S. degree in Electrical Engineering and his Ph.D. degree in Control Engineering from Southeast University, Nanjing, China, in 1988 and 2002, respectively. He has been with Jiangsu University since 1988, where he is presently working as a Professor, and as the Dean of the School of Electrical Information Engineering. From 2003 to 2004, he was a Visiting Professor in the Department of Electronic and Electrical Engineering, University of Sheffield, Sheffield, RNG, UK. His current teaching and research interests include electrical machines, motor drives for electric vehicles and intelligent control. He has authored or coauthored over 200 technical papers and 4 textbooks, and holds 30 patents in these areas. Dr. Liu is a Fellow of the IET.

Yuqi Yang received his B.S. degree in Control Engineering from Jiangsu University, Zhenjiang, China, in 2016, where he is presently working towards his M.S. degree in Control Engineering. His current research interests include the power-electric control of electric machines and high-efficacy control.

Qian Chen (M'16) received his B.S. degree in Electrical Engineering and his Ph.D. degree in Control Engineering from Jiangsu University, Zhenjiang, China, in 2009 and 2015, respectively. He has been with Jiangsu University since 2015, where he is presently working as an Associate Professor in the School of Electrical Information Engineering. His current research interests include electric machine design, modeling, fault analysis and intelligent control.